Seeding the Self-Assembly of DNA Origamis at Surfaces

Huan H. Cao,† Gary R. Abel, Jr.,† Qufei Gu,‡ Gloria-Alexandra V. Gueorguieva,† Yehan Zhang,† Warren A. Nanney,† Eric T. Provencio,† and Tao Ye*,†,‡

†Chemistry and Chemical Biology, University of California, Merced, California 95343, United States
‡Materials and Biomaterials Science and Engineering, University of California, Merced, California 95343, United States

ABSTRACT: Unlike supramolecular self-assembly methods that can organize many distinct components into designer shapes in a homogeneous solution (*e.g.*, DNA origami), only relatively simple, symmetric structures consisting of a few distinct components have been self-assembled at solid surfaces. As the self-assembly process is confined to the surface/interface by mostly nonspecific attractive interactions, an open question is how these interfacial interactions affect multicomponent self-assembly. To gain a mechanistic understanding of the roles of surface environment in DNA origami self-assembly, here we studied the oligonucleotide-assisted folding of a long single-stranded DNA (ssDNA scaffold) that was end-tethered to a dynamic surface, which could actively regulate the DNA-surface interactions. The results showed that even weak surface attractions can lead to defective structures by inhibiting the merging of multiple domains into complete structures. A combination of surface anchoring and deliberate regulation of DNA-surface interactions allowed us to depart from the existing paradigm of surface confinement *via* nonspecific interactions and enabled DNA origami folding to proceed in a solution-like environment. Importantly, our strategy retains the key advantages of surface-mediated self-assembly. Moreover, surface-anchored oligonucleotides could sequence-specifically initiate the growth of DNA origamis of specific sizes and shapes. Our work enables information to be encoded into a surface and expressed into complex DNA surface architectures for potential nanoelectronics and nanophotonics applications. In addition, our approach to surface confinement may facilitate the 2D self-assembly of other molecular components, such as proteins, as maintaining conformational freedom may be a general challenge in the self-assembly of complex structures at surfaces.

KEYWORDS: DNA nanotechnology, DNA origami, self-assembly, supramolecular self-assembly, biomolecular surface chemistry, force spectroscopy, atomic force microscopy

Supramolecular self-assembly at solid surfaces[1] employs intermolecular and molecule-surface interactions to organize molecular components into small clusters, 1D/2D periodic structures,[2-5] quasi-crystalline,[6] and even fractal patterns.[1,6] Self-assembly at surfaces has numerous appeals, including compatibility with *in situ imaging*, ease of purification, and the potential to integrate with top down approaches for device applications.[2,3,7] However, the predictable formation of complex structures at surfaces has been a formidable challenge. For

example, although a ssDNA scaffold can be folded into designer DNA origami structures[8] through base-pairing interactions with hundreds of complementary oligonucleotide "staples",[8,9] studies indicated that once the DNA scaffolds were deposited onto a solid support, they could no longer be properly folded into complete DNA origami structures.[10,11] The growth of DNA origami was only observed at the solid-liquid interface if most of the scaffold had been folded in the solution before surface deposition.[10] As the self-assembly process is confined to the surface/interface by mostly nonspecific attractive interactions,[1] an open question is how these interfacial interactions affect multicomponent self-assembly. DNA nanostructures have been traditionally immobilized onto mica[4,12] or supported lipid bilayers[13] with divalent-cation-mediated nonspecific interactions. Such nonspecific interactions have been difficult to probe and control. If the interactions are weakened to facilitate lateral reorganization, these DNA structures may irreversibly dissociate from the solid support and diffuse away. Moreover, the strengths of interactions were only qualitatively inferred from atomic force microscopy (AFM) images in existing studies.[12,14] Hence, it remains unclear to what extent these interactions hinder DNA origami self-assembly by impeding the reorganization of molecular components, or if they facilitate the formation of 2D structures, as has been reported in the studies of simple, symmetric DNA structures on surfaces.[4,12,15] The lack of understanding of the roles of surface interactions in multicomponent DNA self-assembly has hindered further attempts to construct more complex structures at surfaces.

Here we studied how interfacial interactions influence the DNA origami self-assembly by tethering DNA scaffolds to a carboxyl-terminated self-assembled monolayer (SAM) on a gold support, which allowed us to precisely modulate the DNA-surface interactions between attractive and repulsive regimes without irreversible desorption.[16] After the tethered scaffold interacted with the staples, strong surface interactions were temporarily switched on to immobilize intermediate structures for high-resolution AFM characterization. By examining the folding yields and the populations of intermediate structures under different conditions, we were able to quantify the impact of the surface and optimize the folding process.

RESULTS AND DISCUSSION

Tethering ssDNA Scaffolds to Solid Supports. The substrate used was an ordered 11-mercaptoundecanoic acid (MUDA) SAM on a single-crystal Au(111) support.[16] To tether a DNA scaffold to SAMs, a sticky end appended to the 5' end of the scaffold was hybridized with the 3'-end of a thiolated ssDNA anchor strand (Figure 1a, I & II) in a hybridization buffer containing 1 M NaAc and 1 × TAE.[17] After each step, the surface was rinsed with a buffer solution and submerged in a 5 mM Ni^{2+} solution to immobilize the DNA for AFM imaging (Methods). Consistent with our previous study on this surface,[17] thiolated ssDNA anchors appeared as small protrusions approximately 0.5-1.0 nm in height (Figure 1b), while the surface-tethered ssDNA scaffolds displayed random-coil structures approximately 1.0-1.5 nm in height (Figure 1c, cyan arrow).

DNA Origami Folding under Mg^{2+}. Folding of surface-tethered ssDNA scaffolds was carried out isothermally in a DNA staple buffer solution containing 40% formamide (Figure 1a, III), which helps suppress the adverse secondary structure formation and anneal the folding.[18] The effect of the surface on DNA origami self-assembly was investigated by comparing the folding of free (untethered) scaffolds in a homogeneous solution to folding of

tethered scaffolds. Structures formed from both tethered and untethered scaffolds were both immobilized on the surface at specified time points for AFM characterization (Methods). We found that in a folding solution containing the staples, 12.5 mM Mg^{2+} and 40% formamide, 33.5 ± 2.4% (N = 8 samples) of the untethered scaffolds were folded into the designed rectangular shape in 90 min (Figure 2a, top). In contrast, when tethered scaffolds were exposed to an identical solution, no folded structures could be observed (Figure 2a, bottom). These results suggest that the Mg^{2+}-mediated attractive interactions between DNA and negatively charged surfaces (such as mica and carboxyl terminated SAMs[12,14]) impede the self-assembly of DNA origami confined to the surface.[19]

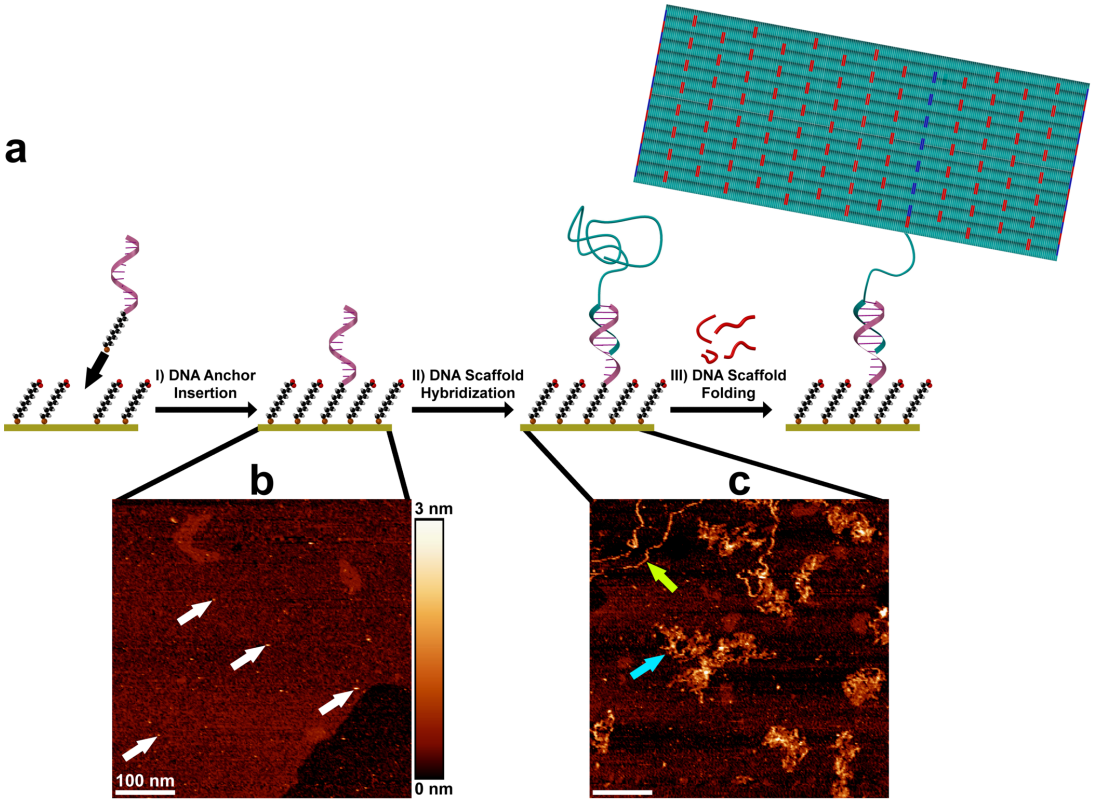

Figure 1. Schematic illustrating self-assembly of DNA origami tethered to a MUDA SAM. (a) A DNA anchor strand is inserted into a MUDA SAM and hybridized with a ssDNA scaffold, which is then incubated with a formamide buffer solution containing DNA staples to initiate folding. Red and blue marks on the DNA origami drawing represent DNA staple and scaffold crossovers, respectively. (b), (c) Representative AFM images resolving the inserted DNA anchors (b, white arrows) and the surface-captured ssDNA scaffolds (c, cyan arrow) on the MUDA SAM. As the yield of the exonuclease digestion used to produce the single stranded scaffolds from dsDNA is below 100%, a few dsDNA scaffolds are also hybridized with the anchor strands on the MUDA SAM (c, green arrow).

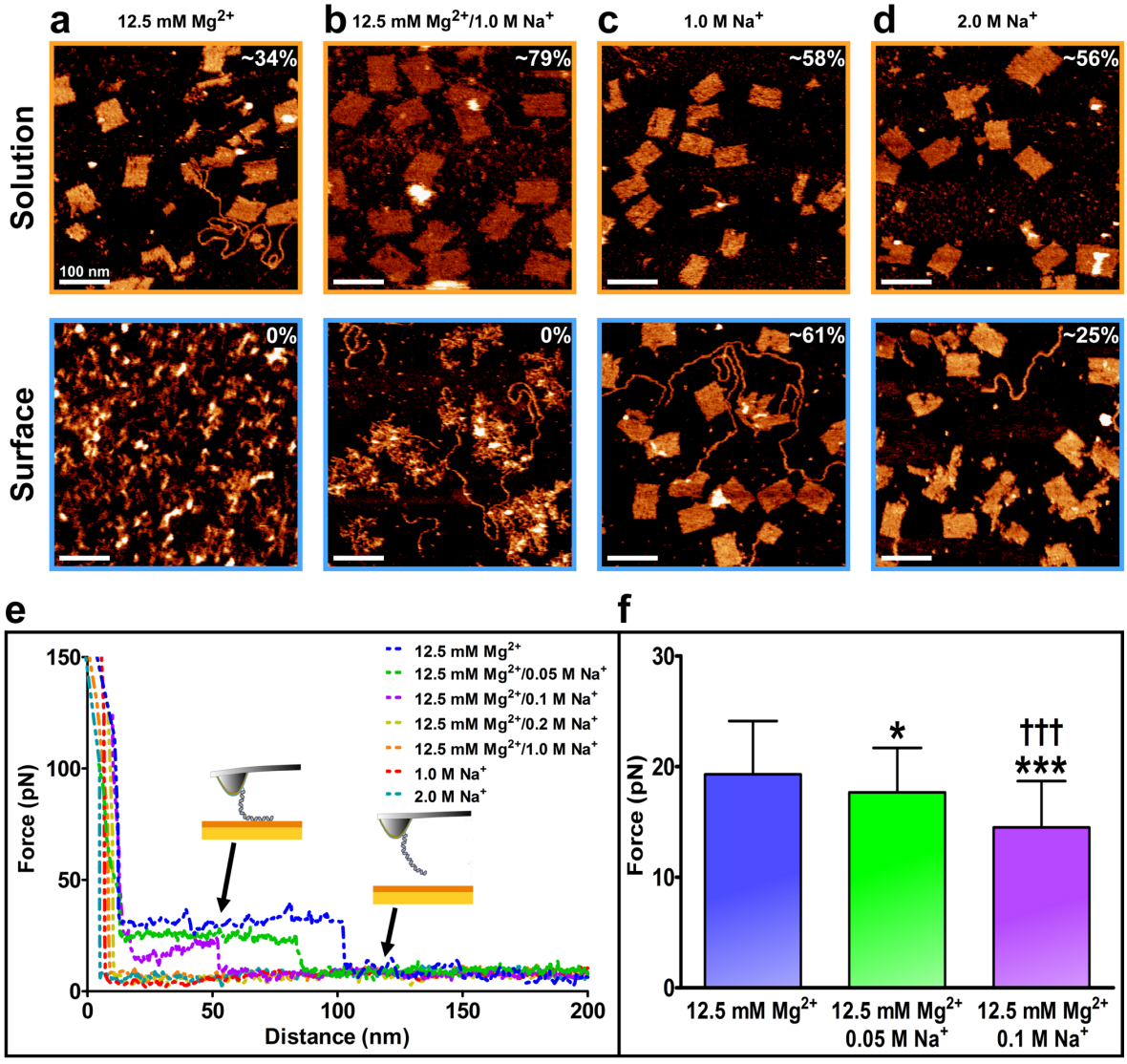

Figure 2. DNA origami self-assembly in the solution phase *vs.* at the surface. (a)-(d) Representative AFM images of the products of staple-assisted folding from the untethered (free) (a, b, c, d, top) and tethered (a, b, c, d, bottom) scaffolds. The structures assembled in a homogeneous solution were deposited on mica for AFM imaging. Average folding yield is reported on the top right corner of AFM images. The Z-height range of AFM images is 0 – 3.0 nm. (e) Representative force/distance curves from SMFS measurements of dsDNA on MUDA SAMs. Force plateaus are decreased in height due to weaker surface interactions as more Na^+ is mixed with Mg^{2+}. (f) Average DNA adhesion force on MUDA SAMs reflects the similar decreasing trend observed in (e). Mean force values are significantly different across groups [$F(2,331) = 32$; $P < 0.001$].*$P < 0.05$ & ***$P < 0.001$ *vs.* 12.5 mM Mg^{2+}, and $^{\dagger\dagger\dagger}P < 0.001$ *vs.* 12.5 mM Mg^{2+}/0.05 M Na^+. Error bars represent standard deviations with $N = 190$, 65, & 79 counts for the 12.5 mM Mg^{2+}, 12.5 mM Mg^{2+}/0.05 M Na^+, and 12.5 mM Mg^{2+}/0.1 M Na^+ conditions, respectively. All conditions tested here include 40% formamide. All of the SMFS measurements were obtained with the same AFM cantilever to eliminate uncertainty associated with force constant calibration.

Quantifying DNA-Surface Interactions. To quantify the strength of DNA-surface interactions, we performed single-molecule force spectroscopy (SMFS) to measure the adhesion forces between the MUDA surface and individual double-stranded (dsDNA) molecules attached to the AFM tip, which serve as a proxy for the partially assembled DNA origami. When using the AFM tip to repeatedly adsorb and detach single DNA molecules from the MUDA surface under different buffer conditions (Methods & Supporting Information Notes S1), we observed force plateaus, which suggest that the adsorbed molecules were peeled off the surface under a quasi-equilibrium condition (Figure 2e, blue curve).[20] Assuming an inter-base distance of 0.32 nm/bp, the measured force of 19.3 ± 4.8 pN (N = 190 counts, Figures 2f & Supporting Information Figure S1a) corresponds to an adsorption energy (E_{ad}) of 1.59 ± 0.40 k_BT/bp in a buffer containing Mg^{2+}, which is used to promote staple hybridization with the DNA scaffold in most studies.[8] Moreover, stronger adhesion forces of 26.7 ± 6.5 pN (E_{ad} of 2.20 ± 0.54 k_BT/bp, N = 56 counts) under the identical buffer conditions were observed on mica (Supporting Information Figures S2a,b). Such Mg^{2+}-mediated attractive interactions are strong enough to constrain the scaffold segments and DNA staples from reorganizing in 3D, thereby hindering DNA origami self-assembly. The addition of monovalent cations was reported to weaken the Mg^{2+}-mediated interactions and increase the mobility of DNA nanostructures immobilized on mica due to charge screening and competition for binding sites on the surface.[12] Indeed, SMFS showed that increasing the concentration of Na^+ reduced the attractive interactions on the MUDA surface in the presence of Mg^{2+} (Figure 2e, green & purple curves, Figure 2f, & Supporting Information Figures S1b,c). When [Na^+] exceeded 0.1 M, the adhesion force was reduced to below the detection limit of our SMFS (3.4 pN)[21] (Figure 2e, yellow and orange curves). Although the Mg^{2+}-mediated attractive interactions are weakened in the presence of added Na^+, self-assembly at the surface in a mixture of Na^+ and Mg^{2+} was still hindered (Figure 2b, bottom) in comparison to self-assembly in a homogeneous solution (Figure 2b, top). Folding under salt conditions other than mentioned here was described in Supporting Information Note S2.

DNA Origami Folding under Na^+. The results suggest that the conflicting requirements of surface confinement and conformational freedom are difficult to meet simultaneously for multicomponent supramolecular self-assembly, where extensive structural reorganization of the components is necessary. The specific end-tethering of DNA scaffolds onto a switchable surface[16] may prevent irreversible desorption while also mitigating attractive surface interactions to retain conformational freedom. Thus, we sought to fold the tethered scaffolds in a buffer that contains 1.0 M NaAc and 1 × Tris-Acetate-EDTA (TAE). This monovalent cation buffer imparts significant conformational freedom to end-tethered DNAs by allowing short-range repulsion between the DNA and the negatively charged MUDA SAM.[16,17] Moreover, similarly concentrated Na^+-containing buffer solutions have been used in previous studies to fold untethered scaffolds.[19] Indeed, under these conditions many of the surface-tethered scaffolds were folded into complete structures (Figure 2c, bottom). Furthermore, the folding yields of the surface-tethered scaffolds and untethered scaffolds are indistinguishable at various time points (Figures 2c, 3) up to 3 hours (We also attempted to fold structures for even longer period of time. While the overnight folding yield in solution reaches ~79%, on-surface assembly drops to ~18%, like due to the degradation of SAM upon overnight incubation in the buffer). However, while the folding yields of free scaffolds remained relatively unchanged as the Na^+ concentration reached 2.0 M (Figure 2d, top), the folding yield at the surface decreased (Figure 2d, bottom), suggesting that this high salt level

induced nonspecific surface interactions that hindered the folding (Supporting Information Note S3).

Because changes in the distribution of intermediate structures evolved from untethered[22] and tethered scaffolds signify alterations in the folding pathways, we examined these distributions to further elucidate the influence of surface interactions on DNA origami self-assembly. The distinct types of intermediate structures evolved from the untethered scaffolds (Figure 3, top) suggest that DNA origami folding can proceed *via* different pathways, consistent with previous *ex situ* imaging studies of untethered DNA origami folding.[22,23] Moreover, the observation of many fragmented features suggests that folding domains may grow concurrently within a single structure and the merging of such domains may be a bottleneck in the self-assembly process. Notably, the intermediate structures and their distributions are similar for untethered and tethered scaffolds at different time points (Figure 3 top *vs.* bottom & Supporting Information Figure S6), indicating that surface interactions have relatively small influences on the folding pathways under 1.0 M Na^+ condition. However, this similarity breaks down for folding under 2.0 M Na^+ condition. While the solution-phase folding proceeded similarly regardless of the increased salt concentration (Figure 4, top), folding under 2.0 M Na^+ at the surface produced substantially more fragmented intermediates than in 1.0 M Na^+ (Figure 4, bottom). This observation suggests a likely cause for the lower folding yield at 2.0 M Na^+ observed in Figure 2d (bottom). The higher ionic strength leads to more screening of electrostatic repulsion between DNA and the SAM surface. Hence nonspecific interactions are stronger in 2.0 M Na^+ and are able to trap the folded domains, hindering them from merging to form complete structures. A similar argument could be made to explain for the observation that the population of fragmented species declined more slowly over time for folding at the surface than in the solution phase under 1.0 M Na^+ condition (Figure 3). This could be a consequence of the small folded domains becoming transiently trapped by relatively weak attractive surface interactions (Supporting Information Note S3) or the reduced conformational freedom of the tethered end. Another notable difference was the aggregation of some tethered DNA origamis, which might arise from the close proximity imposed by surface tethering. We observed regions on the surface with a higher local density of scaffolds produced aggregation of DNA origamis due to blunt-end stacking (Figure 5a, green arrows) or possible DNA staple bridging between two neighboring scaffolds (Figures 5b,c, blue arrows). Such aggregation, which was not observed in the folding of untethered scaffolds (Figure 2, top row),[24] shows that the constraint imposed by surface tethering promotes interactions between DNA origamis. Additional differences between folding in the solution phase and at the surface are mentioned in Supporting Information Note S4.

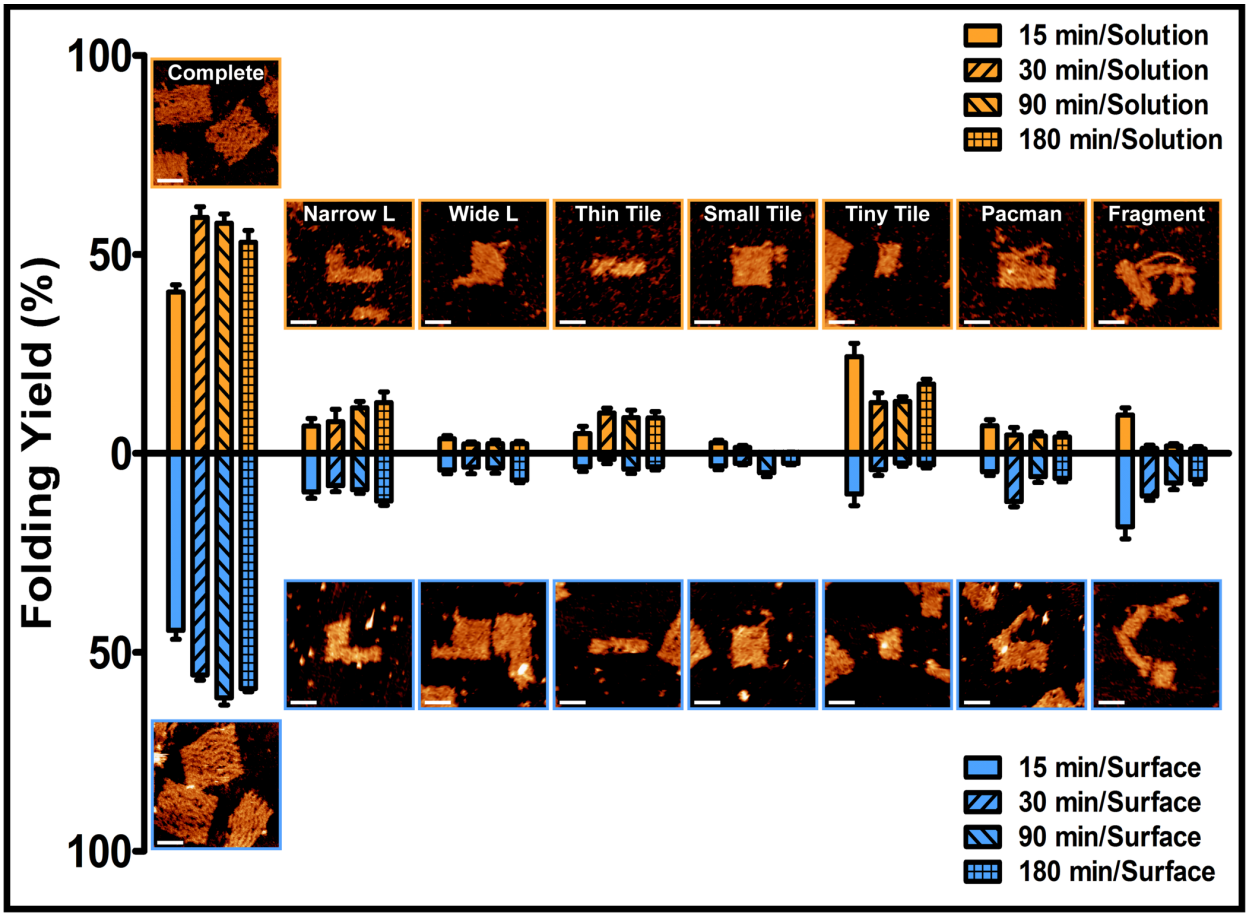

Figure 3. Evolution of intermediate structures folded from untethered scaffolds *vs.* those folded from surface-tethered scaffolds under 1.0 M Na^+. Distribution of well-folded and intermediate structures including their representative AFM images for untethered (top) *vs.* tethered (bottom) scaffolds over different time points. Error bars represent standard errors of the mean with N = 5 – 11 samples per time point. Scale bars are 30 nm with a Z-height range of 0 – 3.0 nm.

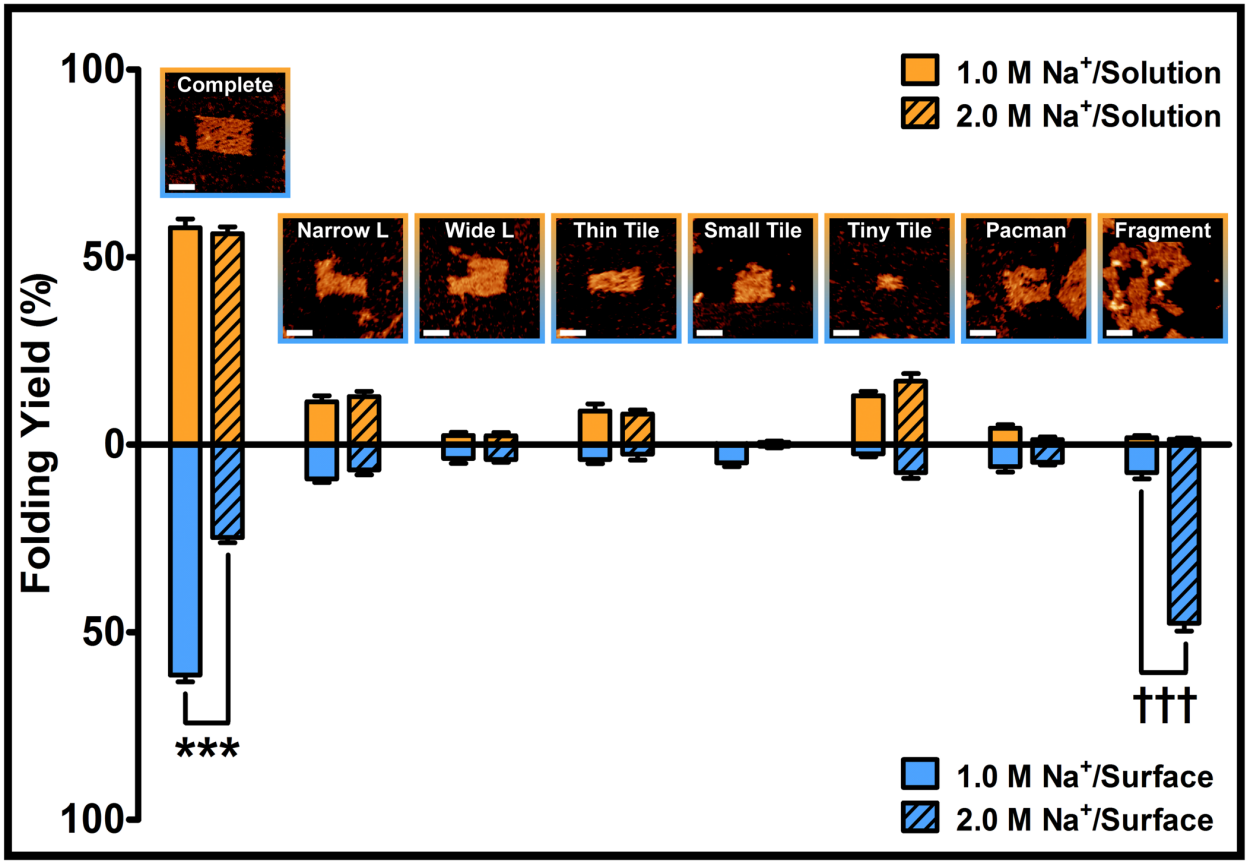

Figure 4. Distribution of well-folded and intermediate structures including their representative AFM images for both untethered and tethered scaffolds under 1.0 and 2.0 M Na^+ conditions. While folding in the solution phase is not sensitive to different salt concentrations, 2.0 M Na^+ condition affects folding at the surface by increasing the population of fragment species and reducing the population of complete structures compared with 1.0 M Na^+ condition. Mean folding yields are similar for the complete structures $t(13) = 0.5$, $P > 0.1$ and the fragmented structures $t(13) = 0.6$, $P > 0.1$ for solution-phase folding. In contrast, mean folding yields are significantly different for the complete structures $t(8) = 16$, $^{***}P < 0.001$ and the fragmented structures $t(8) = 15$, $^{\dagger\dagger\dagger}P < 0.001$ from folding at the surface. Error bars represent standard errors of the mean with $N = 5 – 8$ samples per salt condition. Scale bars are 30 nm with a Z-height range of 0 – 3.0 nm.

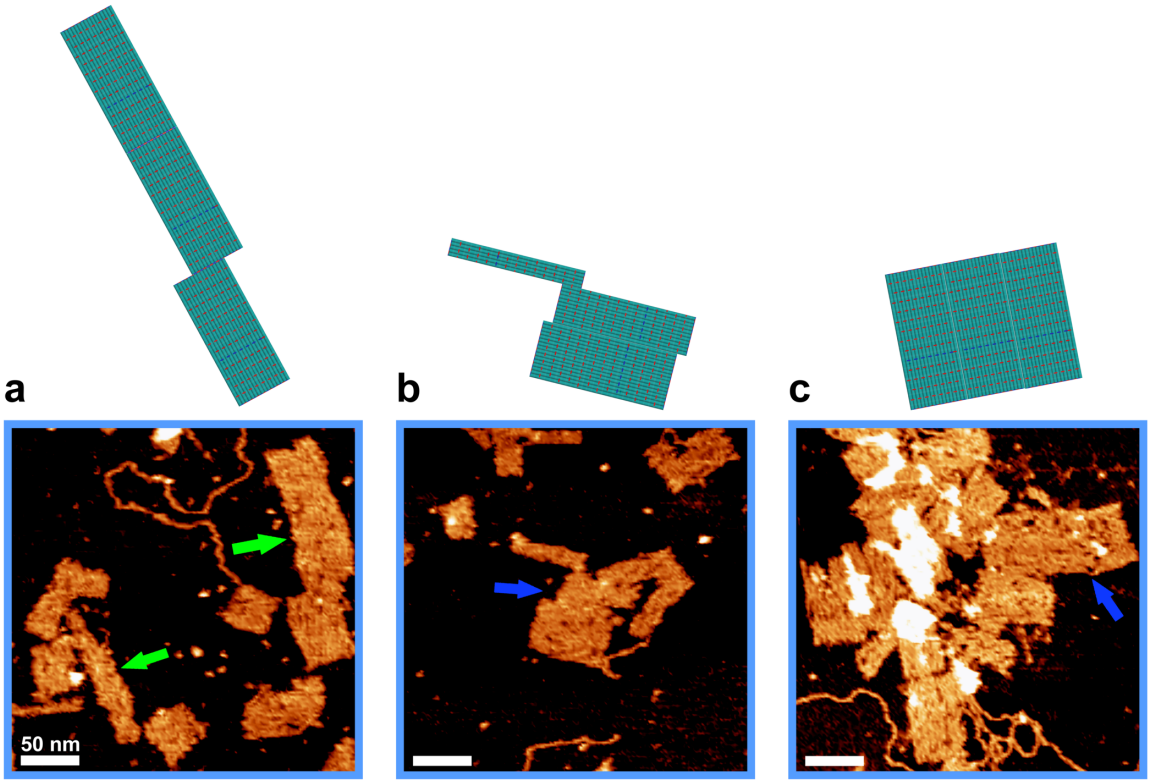

Figure 5. Local crowding of tethered DNA scaffolds promotes aggregation of DNA origami structures. (a)-(c) Schematics (top) and representative AFM images (bottom) display examples of blunt-end stacking (a, green arrows) and possible DNA staple bridging across different folded structures (b & c, blue arrows). The Z-height range of AFM images is 0 – 3.0 nm.

Sequence-Specific Seeding of DNA Origami Folding. Finally, our approach to growing supramolecular complexes at surfaces potentially offers a means of encoding information into the surface to control DNA self-assembly.[4,12,13] Here we performed a preliminary test to assess if different scaffolds can be sequence-specifically captured by the anchor strands and then folded simultaneously and orthogonally into corresponding structures on the same surface. The surface was functionalized with either one or both of two distinct "seed" strands, RSd and CSd (Figure 6, I), which were complementary to the 5' ends of the scaffold strands, RSc and CSc, respectively. When combined with the corresponding sets of staples, the RSc and CSc scaffolds can be folded into the respective rectangular (RE) and cross-shaped (CS) structures. After three different surfaces (RSd only, CSd only, and RSd + CSd) were incubated with a solution containing both the RSc and CSc scaffolds (Figure 6, II), and then with a solution containing both sets of DNA staples (Figure 6, III), we observed the emergence of different DNA origami structures. RSd-seeded surfaces produced predominantly RE origamis, while CSd-seeded surfaces led to CS origamis; the presence of both seeds led to a mix of both RE and CS structures (Figure 6, IV-V). Hence, our approach to seeding the self-assembly at surfaces provides a mechanism to express the information encoded in single molecules (seed strands) into DNA nanostructures of designed size and geometry.

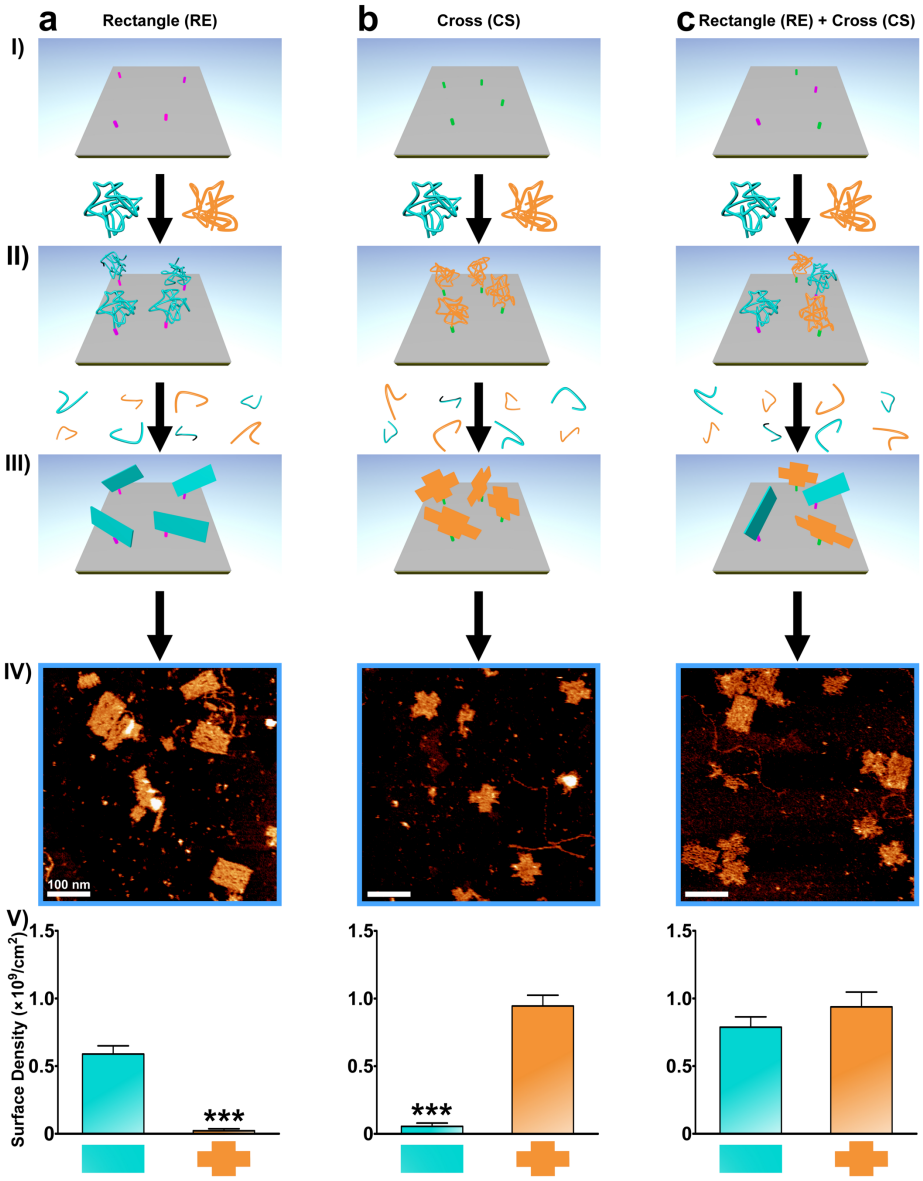

Figure 6. Seeding distinct DNA origami shapes on the same surface. (a)-(c) Schematics and representative AFM images showing the self-assembly of DNA origami rectangles (RE) (a), DNA origami crosses (CS) (b), and both structures (c) on MUDA SAMs. Seeding of DNA origamis starts with the insertion of anchor strands into SAMs (I), followed by the selective capture of ssDNA scaffolds (II), which initiated the growth of DNA origamis (III) shown with the corresponding representative AFM images (IV). The Z-height range for AFM images is 0 – 3.0 nm. (V) Surface densities of completely folded structures on different surfaces. Significantly more RE *vs.* CS species [$t(16) = 9$, $^{***}P < 0.001$] were detected on SAMs decorated with RSd seeds (left), while fewer RE *vs.* CS species [$t(16) = 11$, $^{***}P < 0.001$] were detected on SAMs decorated with CSd seeds (middle). However, similar surface density of RE *vs.* CS species [$t(14) = 1$, $P > 0.1$] were detected on SAMs decorated with both RSd and CSd seeds (right). Error bars represent standard errors of the mean with $N = 8 – 9$ samples per group.

CONCLUSIONS

Our study of DNA origami self-assembly at surfaces highlights the importance of understanding and managing interfacial interactions in forming complex supramolecular structures at surfaces. Future improvements in the stability of SAMs,[25] covalent anchoring of scaffolds,[17] and reduction of nonspecific interactions[26] could improve the yield for tethered DNA origami nanostructures. Surface-seeded self-assembly may allow sophisticated information encoded into specific interactions at the surface to direct the self-assembly of complex surface architectures. Top-down methods that pattern anchor strands[27,28] can initiate the site-specific growth of tethered DNA origamis in spatial proximity, which will enable these structures to connect to form complex hierarchical structures that are difficult to form in the solution phase. The seeded self-assembly can also be adapted for DNA bricks[9] and algorithmic self-assembly of DNA.[29] In addition, our approach may facilitate the self-assembly of other types of building blocks, such as proteins,[5] into complex 2D structures, as the paradoxical demands of conformational freedom and surface confinement are likely a general barrier.

METHODS

Preparation of Thiolated DNA Anchor Strands. All DNA anchor strands were synthesized and then purified using reversed-phase high-performance liquid chromatography by LGC Biosearch Technologies Inc. (Petaluma, CA, US). The DNA products arriving in the lyophilized form were dissolved in ultrapure water (resistivity ≥ 18.0 MΩ · cm) from the Barnstead Nanopure system (Thermo Fisher Scientific, Houston, TX, US) to make 200 μM stock solutions. The DNA solutions were stored at -20 °C. Additionally, the stock solutions of the DNA anchor strands were backfilled with nitrogen gas (Airgas, Radnor Township, PA, US) before storage. Because the anchor strands arrived in the disulfide forms, they needed to be reduced to the thiol forms prior to molecular insertion into SAM defects. A 1 μM of DNA anchor strand was incubated with 1 mM Tris(2-carboxyethyl)phosphine hydrochloride (TCEP) (Millipore-Sigma, St. Louis, MO, US) in an aqueous solution to reduce the disulfides. The solution was backfilled with nitrogen gas and kept in the dark for 30 min at room temperature to minimize thiol oxidation. The anchor strands were then purified with QIAquick nucleotide removal kit (QIAGEN Inc., Santa Clarita, CA, US) and were ready for SAM insertion.

Generation and Amplification of dsDNA Scaffolds. All DNA primers were purchased from Integrated DNA Technologies Inc. (Coralville, IA, US) in the lyophilized form. Stock solutions of DNA primers were prepared and stored as mentioned above. The forward primers were designed to contain a propyl spacer phosphoramidite (iSpC3) that prevents the polymerase from copying over the sticky ends, which are used to hybridize with the anchor strands.[17] They are also modified with an internal DeoxyUridine (ideoxyU) to enable the downstream uracil-DNA glycosylase (UDG) reaction.[30] The reverse primers were phosphorylated at the 5' end to enable exonuclease digestion.[31] All dsDNA templates including the circular M13mp18 RF I phage vector (Cat. # N4018S) and the linear pTXB1 vector (Cat. # N6707S), and all enzymes/accompanied buffers used in polymerase chain reaction (PCR), template linearization, UDG cleavage, and digestion of complementary DNA strands were purchased from New England Biolabs Inc. (Ipswich, MA, US). To use the phage

vector for PCR, circular M13mp18 RF I templates needed to be linearized. A 10 ng/μL M13mp18 RF I was mixed with 20 units of Eco RI enzyme, 1 × Eco RI buffer (Cat. # R0101S), and 200 μg/μL BSA (Cat. # B9000S) in a 50-μL aqueous solution, which was incubated at 37 °C for 2 h to linearize the phage vector, heated up to 65 °C for 20 min to denature the enzymes, and cooled to 4 °C in an MJ Mini Personal Thermal Cycler (Bio-Rad Laboratories Inc., Hercules, CA, US). The linearized DNA templates were purified with the QIAquick PCR Purification Kit (QIAGEN Inc., Santa Clarita, CA, US). The concentrations of our DNA samples were calculated by measuring the optical absorption at 260 nm with a Nanodrop-1000 spectrophotometer (Thermo Fisher Scientific, Marietta, OH, US).

For PCR amplification, either 50 pg/μL of linearized M13mp18 RF I or 1 ng/ μL of linear pTXB1 dsDNA template was mixed with 200 nM of forward/reverse primers and OneTaq 1 × master mix with standard buffer (Cat. # M0482S) in a 50-μL aqueous solution. The dsDNA scaffolds were PCR-amplified in the MJ Mini Personal Thermal Cycler according to the following thermal program: 95 °C for 3 min, [95 °C for 3 s, 53 °C for 45 s, 72 °C for 4 min (for 3655 bp from M13mp18 RF I), 2 min 30 s (for 1031 bp from M13mp18 RF I), or 3 min 30 s (for 2581 bp from pTXB1)] × 34 cycles, 72 °C for 10 min, and holding indefinitely at 4 °C. The PCR products were then purified with the QIAquick PCR Purification Kit. The 3655- & 2581-bp scaffolds were used for folding 76 × 47 nm^2 DNA rectangles and 65 × 59 nm^2 DNA crosses, respectively.

Generation of ssDNA Scaffolds. To remove complementary DNA strands from PCR-amplified dsDNA scaffolds, ∼30 nM (for M13mp18 RF I) or 80 nM (for pTXB1) of dsDNA scaffold was mixed with 40 units of lambda exonuclease, and 1 × lambda exonuclease reaction buffer (Cat. # M0262S) in a 50-μL aqueous solution. The mixture was incubated at 37 °C for 6 h to digest the complementary strands,[31] heated up to 75 °C for 10 min to denature the enzymes, and cooled to 4 °C in the MJ Mini Personal Thermal Cycler. The enzyme-digested ssDNA scaffolds were then purified with the QIAquick PCR Purification Kit. Due to the incomplete exonuclease digestion, we also observed the remaining undigested dsDNA scaffolds as seen in Figures 1C; 2B, C, D (bottom row); 5A, B, C; and 6(IV).[32-34]

DNA Origami Folding of Untethered Scaffolds in the Solution Phase. Each DNA staple (Integrated DNA Technologies Inc., Coralville, IA, US) arrived as 100 μM in 10 mM Tris (tris(hydroxymethyl)aminomethane), 0.1 mM ethylenediaminetetraacetic acid (EDTA) solution in 96-well plates. The DNA staples were then mixed together in an aqueous solution containing 40 mM Tris-acetate, 1 mM EDTA, pH 8.3 (1 × TAE) (Fisher Scientific, Mfr.# FLBP13321, Houston, TX, US) to make stock solutions of 1 μM and stored at -20 °C. Folding was carried out by incubating an aqueous solution of 5 nM untethered DNA scaffold, 25 nM for each DNA staple, 1.0 M NaAc, 1 × TAE, and 40% formamide[24] for a specified time duration in the dark at room temperature. The reaction volume was 30 or 50 μL. The same folding procedure was used for folding experiments under different salt conditions.

Preparation of Mica Substrates. Highest grade V1 20-mm mica discs (Ted Pella Inc., Redding, CA, US) were freshly cleaved with a packaging tape and incubated with an aqueous solution of either 5 mM $NiAc_2$, 0.1 × TAE or 20 mM $NiAc_2$, 0.1 × TAE if folding was done in $MgAc_2$ or NaAc, respectively for 2 min. When the folding solution was added to mica substrates, an aqueous solution of 12.5 mM $MgAc_2$, 0.1 × TAE (folding in $MgAc_2$) or 20 mM $NiAc_2$, 0.1 × TAE (folding in NaAc) was also immediately added. After 1-min incubation, the

substrates were incubated with the same respective aqueous solution for another 1 min and then placed in the imaging buffer (5 mM $NiAc_2$, 0.1 × TAE).

Preparation of Dynamic SAMs. All chemical reagents and buffer solutions were purchased from Fisher Scientific (Houston, TX, US) unless otherwise stated. To ensure reasonable cleanliness, all glassware was cleaned with piranha solutions prior to use. **CAUTION:** piranha solutions (3:1 (v/v) sulfuric acid to hydrogen peroxide) are highly corrosive and react violently with organic compounds. Proper personal protective equipment is needed. Well-ordered SAMs on Au beads (Scientific Instrument Services Inc., Ringoes, NJ, US) with single-crystal facets were prepared following previously reported protocols.[16,17,35] The substrates were rinsed and sonicated with acetone for 1 min and with methanol for another 1 min. After immersing in hot (120 °C) nitric acid for 25 min, the substrates were rinsed thoroughly with ultrapure water and blown dry with filtered air. Hydrogen gas was used to flame anneal the Au beads, which were then immersed in an ethanolic solution containing 10% acetic acid by volume and 1-2 mM of MUDA (Millipore-Sigma, St. Louis, MO, US). The thiol solution was then backfilled with nitrogen gas (Airgas, Radnor Township, PA, US), sealed with parafilm, and kept in the dark for 16-24 h at room temperature to minimize thiol oxidation.

DNA Anchor Strand Insertion, ssDNA Scaffold Hybridization, and Formamide-Assisted Folding at the Surface. After SAM formation, the substrates were quickly rinsed and sonicated with an ethanolic solution containing 10% acetic acid by volume for 5 sec. After thorough rinsing with ultrapure water and blowing dry with filtered air, the substrates were placed in a home-made polytetrafluoroethylene liquid cell on an AFM stage and rinsed with a 1 × TAE solution several times. Insertion of anchor strands was then carried out by incubating the MUDA SAM with an aqueous solution containing 1.0 μM of purified, thiolated DNA strand, 50 mM NaAc, 1 × TAE, and 1 mM TCEP for 20-30 min. The substrates were then rinsed 3 times with a 1 × TAE solution by pipetting the solution up/down, directly on the Au beads several times. Following the insertion step, an aqueous solution of 1.0-2.0 nM ssDNA scaffold, 1.0 M NaAc, and 1 × TAE was incubated with the Au beads for 30 min. The substrates were then rinsed 6 times with a 0.8 M NaAc, 1 × TAE solution (rinsing buffer). Following the rinsing, the substrates were incubated with an aqueous solution containing 25 nM for each DNA staple, 1.0 M NaAc, 1 × TAE, and 40% formamide for a specified amount of time in the dark at room temperature to initiate the folding of the surface-tethered scaffolds. The substrates were then rinsed 3 times with the rinsing buffer and immersed in the imaging buffer for AFM characterization. This same procedure was also used to conduct folding experiments under other salt conditions.

Formamide-Annealed Folding at the Surface. This procedure was used for surface-seeded folding of DNA rectangles and crosses at MUDA SAMs. Insertion of DNA anchor strands, ssDNA scaffold hybridization, and formamide-assisted folding on MUDA SAMs were prepared according to the instruction given in the previous paragraph. The substrates were then rinsed 3 times with the rinsing buffer and incubated with another folding solution (1.0 M NaAc, 1 × TAE) of lower formamide percentages (*e.g.* 35%) and higher DNA staple concentration (50 nM/staple) for a specified time duration. This step was repeated one more time with another folding solution of 30% formamide and 50 nM for each DNA staple. After rinsing 3 times with the rinsing buffer, the substrates were immersed in the imaging buffer for AFM characterization. For each rinse after ssDNA scaffold hybridization and folding, the solution was pipetted to the side of the Au bead and immediately withdrawn to minimize

possible damages to surface-hybridized DNAs arising from the physical rinsing step. To remove excess ssDNA scaffolds nonspecifically adsorbed on SAMs, 1 × TAE buffered solution with a lower salt concentration (0.2 M instead of 0.8 M NaAc) was used (See Note S3).

Important Note to Surface Treatment. All solution incubation steps were done at room temperature (23 °C) and in the dark to minimize thiol oxidation. It is essential that the Au beads are continuously exposed to an aqueous solution during DNA insertion, scaffold hybridization, and folding steps. For example, when the reaction solution is removed, the substrate is immediately immersed in the rinsing solution.

AFM Imaging. All AFM images were collected under the imaging buffer at room temperature. The AFM probes (Model SNL-10, Bruker Nano Inc., Santa Barbara, CA, US) with nominal spring constants of 0.35 (tip A) or 0.24 (tip C) N/m were used for tapping-mode imaging with our NTEGRA AFM (NT-MDT America, Tempe, AZ, US). All images were collected using the Nova software (version 1.1.0.1903) at a resolution of 512 × 512 pixel^2, a scan rate of 0.7-1.3 Hz, a driving frequency of 13-15 kHz, and a driving amplitude of ~30 – 50 nm.

AFM Image Analyses and Challenges. All images were processed with WSxM software version 5.0.[36] The folding yield was analyzed manually using Gimp version 2.8 (a free online software).[37] The intermediate structures were counted based on their distinct shapes and then grouped into different shape categories (Table S1 & Figure S11). Any surface features with dimension < 15 × 15 nm^2 were not counted because they did not adopt any well-defined shape belonging to our shape categories. Moreover, any surface features with topographical height > 2.5 nm were not counted (and regarded as surface contaminations) unless their shapes could be recognized as belonging to our shape categories. As seen in Figure 5C, aggregation of folded/partially folded structures on the surface could cause one structure to lay on top of neighboring structures yielding a topographical height > 2.5 nm. As a result, the structures on the top might not be strongly immobilized under Ni^{2+} and thus difficult to identify. However, in cases where the shape of the top structures could be visualized, they were counted and categorized. Additionally, fragments of structures could appear to belong to the same scaffolds or they could stem from different scaffolds lying next to each other on the surface. If the structures could be well-differentiated from their neighbors, they would be placed into one of the shape categories. Otherwise, they would not be counted. Thus, counting and categorizing intermediate structures from their aggregation on surfaces might contribute some errors to the overall folding yield estimation. We are currently developing an imaging recognition algorithm to assist with detecting and segmenting the specific shapes of intermediate structures to improve our capability of quantifying the folding yield on surfaces.

Preparation of DNA Anchor Strands and Scaffold Sticky Ends for Hydrazone Crosslink in SMFS Experiments. The interstrand hydrazone-crosslinking follows a previously established protocol.[30] DNA anchor strands were designed to carry an internal deoxycytidine (dC), which was modified with an amine group. 40 μM of anchor strands was mixed with 0.3 M $NaHSO_3$, 0.1 M phosphate buffered saline (PBS) ([NaCl] = 0.005 M, pH 5.0), and 4.0 M hydrazine in a ~25-μL aqueous solution. The solution was backfilled with nitrogen gas, heated at 50 °C for 3 h to modify the dC moiety with an amine group, and then cooled to 4 °C in the MJ Mini Personal Thermal Cycler. After the amine modification, the reaction solution was mixed with a 75-μL aqueous solution containing 0.1 M Tris hydrochloride,

0.01 M triethylamine, and 0.001 M EDTA to quench any remaining unreacted reactants. The sample was then purified with the QIAquick nucleotide removal kit.

The sticky ends of PCR-amplified dsDNA scaffolds carry a dU moiety, which could be cleaved by UDG enzymes to generate an abasic site. 30 nM (for M13mp18 RF I) or 150 nM (for pTXB1) of PCR-amplified dsDNA was mixed with 5 units of UDG enzyme and 1 × UDG Reaction Buffer (Cat. # M0280S) in a 50-μL aqueous solution, which was incubated at 37 °C for 1 h to create the abasic sites, and then cooled to 4 °C in the MJ Mini Personal Thermal Cycler. The modified dsDNA scaffolds were purified with the QIAquick PCR Purification Kit.

Preparation of AFM Probes for SMFS Experiments. Several Au-coated Si AFM tips (Model NPG-10, Bruker Nano Inc., Santa Barbara, CA, US) were cleaned by first exposing the tips to the ultraviolet (UV) radiation for 20 min to remove organic contaminants and then immersing them in hot ethanol at 77-78 °C for another 20 min to reduce oxidized Au due to the UV exposure. To decorate the Au-coated tips with DNAs, they were incubated with an aqueous solution containing 50 nM purified, thiolated DNA anchor strand, whose cytosine base has been amine-modified (See the previous paragraph), 50 mM NaAc, 2 mM $MgAc_2$, 1 × TAE, and 2 mM TCEP in a Teflon beaker for 1 h, followed by rinsing 3 times with the 1 × TAE solution. The tips were then immersed in a 1 mM ethanolic solution of 11-mercaptoundecanol (MCU) (Millipore-Sigma, St. Louis, MO, US) for 2 h. "Backfilling" the tips with MCU was used to minimize nonspecific adsorption of DNAs on Au surfaces from the previous step.[38] Following MCU backfill, the tips were rinsed 3 times with the 1 × TAE solution and then incubated with an aqueous solution of 50 nM 1031-bp dsDNA scaffold, whose sticky end composed of an abasic site (See the previous paragraph), 1M NaAc, 2 mM $MgAc_2$, 1 × TAE, and 1 mM SDS in a Teflon beaker for 1 h. The dsDNA scaffolds used here were 1031 bp in length and PCR-amplified from the linearized M13mp18 RF I dsDNA template. After scaffold hybridization, the tips were then rinsed 3 times with the rinsing buffer and placed in a beaker containing the 0.05 M PBS ([NaAc] = 0.1 M, pH 5.0) solution, which was heated up to ~50 °C for 10 min on a hot plate to form the interstrand crosslink between DNA anchor strands and scaffolds.[30] The whole setup was then cooled to room temperature.

Measuring DNA-SAM Interactions with SMFS. The substrates (Au bead or mica) were prepared by following the procedures described above. The dsDNA-modified Au tips were used with Keysight 5500 AFM (Keysight Technologies, Santa Rosa, CA, US) under contact mode for SMFS measurement. A loading rate of applied forces on the cantilever, ranging from 300 to 500 pN/s and an approach/retract velocity of 400-500 nm/s, were used to measure DNA adhesion forces on MUDA SAMs or mica substrates under different buffer/salt conditions. A complete tip approach/retract cycle is ~3 s. Force-distance curves were collected with PicoView 2.0 (Keysight Technologies, Santa Rosa, CA, US).

The adhesion force between the DNA scaffold and the surface is proportional to the deflection of the AFM cantilever *via* Hooke's law:

$$F = k \times s \times v \qquad (1)$$

Where k is the spring constant, s is the tip deflection sensitivity, and v is the tip deflection in volts (V). The deflection sensitivity was measured by taking the inverse of the slope of the force-distance curves (nm/V), and the spring constant was calibrated by the thermal noise method[39] using LabView (National Instruments, Austin, TX, US):

$$k = \frac{k_B \mathrm{T}}{<\Delta Z^2>} \qquad (2)$$

where k_B is the Boltzmann's constant, T is the temperature, and ΔZ is the deflection of the cantilever. Force-distance curves for tip retraction showing single plateau or multiple plateaus were used to extract the tip deflection. A MATLAB (MATLAB Inc., Waltham, MA, US) built-in function named edge detection was used to find the boundaries of the plateaus, which was then used to determine the distance between the two plateau edges corresponding to the length of DNAs interacting with the surface. Moreover, the plateau average height in each force-distance curve was used to determine the tip deflection and the adhesion force according to the equation (1) above. Any plateau lengths < 20 nm were excluded as they may arise from brief contact at the distal ends of dsDNAs or nonspecific adsorption of dsDNAs on the AFM tips. An ideal force plateau should be ~335 nm in length, as this corresponds to the contour length of the 1031-bp DNA. However, such ideal length was rarely observed in our experiments; the observed force plateaus were generally < 300 nm in length depending on the applied loading rate, the DNA conjugation chemistry, and the tip geometry. Occasionally, multiple plateaus were observed suggesting that several tip-anchored DNA molecules were peeled off the surface sequentially (Figure S2g). As a result, only the last force plateau was quantified.

Statistical Analyses. Data from SMFS measurements and AFM folding yield experiments were analyzed by one-way analysis of variance, followed by Tukey's multiple group comparisons. Individual group comparisons for SMFS and AFM data were also analyzed by two-tailed, unpaired Student's t-tests. All statistics were implemented using GraphPad Prism (GraphPad Software Inc., San Diego, CA, US). Data for SMFS measurements and AFM experiments are reported as means ± standard deviations and standard errors of the means, respectively, with probabilities of $P < 0.05$ considered statistically significant.

ASSOCIATED CONTENT

A preprint version of the work was submitted to the ChemRxiv preprint server. Cao, H. H.; Abel, G. R. Jr.; Gu, Q.; Gueorguieva, G-A. V.; Zhang, Y.; Nanney, W. A.; Ye, T. *Seeding the Self Assembly of DNA Origamis at Surfaces.* ChemRxiv. Preprint. 2019, 11307779, https://doi.org/10.26434/chemrxiv.11307779.v1 (Accessed Dec. 19,2019).

Supporting Information

The Supporting Information is available free of charge on the ACS Publications website at DOI:

Detailed notes on the effects of formamide on DNA-surface interactions in SMFS experiments, the effects of nonspecific interactions on folding at the surface, additional differences between folding in the solution phase and at the surface, additional SMFS/AFM data over different salt conditions, caDNAno designs, and DNA sequences (PDF).

The authors declare no competing financial interests.

AUTHOR INFORMATION

Corresponding Author

*Email: tao.ye@ucmerced.edu

ORCID
Huan H. Cao: 0000-0002-5301-3134
Tao Ye: 0000-0001-8615-3275

Author Contributions
H.H.C., G.R.A., & T.Y. initiated the project and designed the experiments; H.H.C., G.R.A., Q.G., G.-A.V.G., Y.Z., W.A.N., & E.T.P. performed the experiments; H.H.C., Q.G., G.-A.V.G., & Y.Z. analyzed and interpreted the experimental results; H.H.C. & T.Y. wrote the manuscript with assistance from G.R.A., Q.G., G.-A.V.G., Y.Z., W.A.N., & E.T. P.; and T.Y. guided the project.

ACKNOWLEDGMENTS
This study is supported by National Science Foundation (DMR1410199, and CHE1808213), and Merced nAnomaterials Center for Energy and Sensing (MACES), a NASA MIRO funded research and education center, under award NNX15AQ01. Q.G. acknowledges support by UC Merced BEST Summer Fellowships. W.A.N. acknowledges support by a NASA MUREP fellowship.

REFERENCES

1. Mali, K. S.; Pearce, N.; De Feyter, S.; Champness, N. R. Frontiers of Supramolecular Chemistry at Solid Surfaces. *Chem. Soc. Rev.* **2017,** *46*, 2520-2542.
2. Ruiz, R.; Kang, H. M.; Detcheverry, F. A.; Dobisz, E.; Kercher, D. S.; Albrecht, T. R.; de Pablo, J. J.; Nealey, P. F. Density Multiplication and Improved Lithography by Directed Block Copolymer Assembly. *Science* **2008,** *321*, 936-939.
3. Piva, P. G.; DiLabio, G. A.; Pitters, J. L.; Zikovsky, J.; Rezeq, M.; Dogel, S.; Hofer, W. A.; Wolkow, R. A. Field Regulation of Single-Molecule Conductivity by a Charged Surface Atom. *Nature* **2005,** *435*, 658-661.
4. Sun, X. P.; Ko, S. H.; Zhang, C. A.; Ribbe, A. E.; Mao, C. D. Surface-Mediated DNA Self-Assembly. *J. Am. Chem. Soc.* **2009,** *131*, 13248-13249.
5. Pyles, H.; Zhang, S.; De Yoreo, J. J.; Baker, D. Controlling Protein Assembly on Inorganic Crystals through Designed Protein Interfaces. *Nature* **2019,** *571*, 251-256.
6. Wasio, N. A.; Quardokus, R. C.; Forrest, R. P.; Lent, C. S.; Corcelli, S. A.; Christie, J. A.; Henderson, K. W.; Kandel, S. A. Self-Assembly of Hydrogen-Bonded Two-Dimensional Quasicrystals. *Nature* **2014,** *507*, 86-89.
7. Meyer, R.; Sacca, B.; Niemeyer, C. M. Site-Directed, On-Surface Assembly of DNA Nanostructures. *Angew. Chem. Int. Edit.* **2015,** *54*, 12039-12043.
8. Rothemund, P. W. K. Folding DNA to Create Nanoscale Shapes and Patterns. *Nature* **2006,** *440*, 297-302.
9. Ke, Y. G.; Ong, L. L.; Shih, W. M.; Yin, P. Three-Dimensional Structures Self-Assembled from DNA Bricks. *Science* **2012,** *338*, 1177-1183 .
10. Song, J.; Zhang, Z.; Zhang, S.; Liu, L.; Li, Q.; Xie, E. Q.; Gothelf, K. V.; Besenbacher, F.; Dong, M. D. Isothermal Hybridization Kinetics of DNA Assembly of Two-Dimensional DNA Origami. *Small* **2013,** *9*, 2954-2959.
11. Song, J.; Arbona, J. M.; Zhang, Z.; Liu, L.; Xie, E. Q.; Elezgaray, J.; Aime, J. P.; Gothelf, K. V.; Besenbacher, F.; Dong, M. D. Direct Visualization of Transient Thermal Response of a DNA Origami. *J. Am. Chem. Soc.* **2012,** *134*, 9844-9847.
12. Woo, S.; Rothemund, P. W. K. Self-Assembly of Two-Dimensional DNA Origami Lattices Using Cation-Controlled Surface Diffusion. *Nat. Commun.* **2014,** *5*, 1-9.
13. Suzuki, Y.; Sugiyama, H.; Endo, M. Complexing DNA Origami Frameworks through Sequential Self-Assembly Based on Directed Docking. *Angew. Chem. Int. Edit.* **2018,** *57*, 7061-7065.
14. Hansma, H. G.; Laney, D. E. DNA Binding to Mica Correlates with Cationic Radius: Assay by Atomic Force Microscopy. *Biophys. J.* **1996,** *70*, 1933-1939.
15. Suzuki, Y.; Endo, M.; Sugiyama, H. Lipid-Bilayer-Assisted Two-Dimensional Self-Assembly of DNA Origami Nanostructures. *Nat. Commun.* **2015,** *6*, 1-9.
16. Abel, G. R.; Josephs, E. A.; Luong, N.; Ye, T. A Switchable Surface Enables Visualization of Single DNA Hybridization Events with Atomic Force Microscopy. *J. Am. Chem. Soc.* **2013,** *135*, 6399-6402.

17. Abel, G. R.; Cao, B. H.; Hein, J. E.; Ye, T. Covalent, Sequence-Specific Attachment of Long DNA Molecules to a Surface Using DNA-Templated Click Chemistry. *Chem. Commun.* **2014,** *50*, 8131-8133.
18. Jungmann, R.; Liedl, T.; Sobey, T. L.; Shih, W.; Simmel, F. C. Isothermal Assembly of DNA Origami Structures Using Denaturing Agents. *J. Am. Chem. Soc.* **2008,** *130*, 10062-10063.
19. Martin, T. G.; Dietz, H. Magnesium-Free Self-Assembly of Multi-Layer DNA Objects. *Nat. Commun.* **2012,** *3*, 1-6.
20. Erdmann, M.; David, R.; Fornof, A.; Gaub, H. E. Electrically Controlled DNA Adhesion. *Nat. Nanotechnol.* **2010,** *5*, 154-159.
21. Lekka, M., *Cellular Analysis by Atomic Force Microscopy*. 1st ed.; Pan Stanford Publishing Pte. Ltd.: Singapore, 2017; p 228.
22. Wah, J. L. T.; David, C.; Rudiuk, S.; Baigl, D.; Estevez-Torres, A. Observing and Controlling the Folding Pathway of DNA Origami at the Nanoscale. *ACS Nano* **2016,** *10*, 1978-1987.
23. Dunn, K. E.; Dannenberg, F.; Ouldridge, T. E.; Kwiatkowska, M.; Turberfield, A. J.; Bath, J. Guiding the Folding Pathway of DNA Origami. *Nature* **2015,** *525*, 82-86.
24. Zhang, Z.; Song, J.; Besenbacher, F.; Dong, M. D.; Gothelf, K. V. Self-Assembly of DNA Origami and Single-Stranded Tile Structures at Room Temperature. *Angew. Chem. Int. Edit.* **2013,** *52*, 9219-9223.
25. Li, Z.; Jin, R. C.; Mirkin, C. A.; Letsinger, R. L. Multiple Thiol-Anchor Capped DNA-Gold Nanoparticle Conjugates. *Nuc. Acids Res.* **2002,** *30*, 1558-1562.
26. Blaszykowski, C.; Sheikh, S.; Thompson, M. Surface Chemistry to Minimize Fouling from Blood-Based Fluids. *Chem. Soc. Rev.* **2012,** *41*, 5599-5612.
27. Josephs, E. A.; Ye, T. Nanoscale Positioning of Individual DNA Molecules by an Atomic Force Microscope. *J. Am. Chem. Soc.* **2010,** *132*, 10236-10238.
28. Kufer, S. K.; Puchner, E. M.; Gumpp, H.; Liedl, T.; Gaub, H. E. Single-Molecule Cut-and-Paste Surface Assembly. *Science* **2008,** *319*, 594-596.
29. Barish, R. D.; Schulman, R.; Rothemund, P. W. K.; Winfree, E. An Information-Bearing Seed for Nucleating Algorithmic Self-Assembly. *Proc. Natl. Acad. Sci. USA* **2009,** *106*, 6054-6059.
30. Varela, J. G.; Gates, K. S. A Simple, High-Yield Synthesis of DNA Duplexes Containing a Covalent, Thermally Cleavable Interstrand Cross-Link at a Defined Location. *Angew. Chem. Int. Edit.* **2015,** *54*, 7666-7669.
31. Zhang, H. L.; Chao, J.; Pan, D.; Liu, H. J.; Huang, Q.; Fan, C. H. Folding Super-Sized DNA Origami with Scaffold Strands from Long-Range PCR. *Chem. Commun.* **2012,** *48*, 6405-6407.
32. Han, D. R.; Qi, X. D.; Myhrvold, C.; Wang, B.; Dai, M. J.; Jiang, S. X.; Bates, M.; Liu, Y.; An, B.; Zhang, F.; Yan, H.; Yin, P. Single-Stranded DNA and RNA Origami. *Science* **2017,** *358*, 1-10.
33. Kozyra, J.; Ceccarelli, A.; Torelli, E.; Lopiccolo, A.; Gu, J. Y.; Fellermann, H.; Stimming, U.; Krasnogor, N. Designing Uniquely Addressable Bio-Orthogonal Synthetic Scaffolds for DNA and RNA Origami. *ACS Synth. Biol.* **2017,** *6*, 1140-1149.
34. Kishi, J. Y.; Schaus, T. E.; Gopalkrishnan, N.; Xuan, F.; Yin, P. Programmable Autonomous Synthesis of Single-Stranded DNA. *Nat. Chem.* **2018,** *10*, 155-164.
35. Clavilier, J.; Faure, R.; Guinet, G.; Durand, R. Preparation of Monocrystalline Pt Microelectrodes and Electrochemical Study of the Plane Surfaces Cut in the Direction of the {111} and {110} Planes. *J. Electroanal. Chem.* **1980,** *107*, 205-209.

36. Horcas, I.; Fernandez, R.; Gomez-Rodriguez, J. M.; Colchero, J.; Gomez-Herrero, J.; Baro, A. M. WSXM: A Software for Scanning Probe Microscopy and a Tool for Nanotechnology. *Rev. Sci. Instrum.* **2007,** *78*, 1-8.
37. Kimball, S.; Mattis, P. GNU Image Manipulation Program. https://www.gimp.org/ (accessed Nov. 1, 2019).
38. Herne, T. M.; Tarlov, M. J. Characterization of DNA Probes Immobilized on Gold Surfaces. *J. Am. Chem. Soc.* **1997,** *119*, 8916-8920.
39. Matei, G. A.; Thoreson, E. J.; Pratt, J. R.; Newell, D. B.; Burnham, N. A. Precision and Accuracy of Thermal Calibration of Atomic Force Microscopy Cantilevers. *Rev. Sci. Instrum.* **2006,** *77*, 6.

TOC Graph